51st IEEE Conference on Decision and Control
December 10-13, 2012. Maui, Hawaii, USA

Validation of a nonlinear reactive control law for three-dimensional particle tracking in confocal microscopy

Trevor T. Ashley†, Catherine Chan-Tse⋆, and Sean B. Andersson†‡
† Dept. of Mechanical Engineering, ⋆ Dept. of Electrical and Computer Engineering, ‡ Division of Systems Engineering
Boston University, Boston, MA 02215 USA
{tashley,cchantse,sanderss}@bu.edu

Abstract— **A nonlinear control law for reactively tracking a diffusing fluorescent particle in three dimensions is reviewed and preliminary experimental results are presented. The control law, originally derived in the context of exploring scalar potential fields, converges to a volume around the maximum of the point spread function of a confocal microscope using very little information of the underlying structure of the field. Experimental results show the control law can track particles with diffusion coefficients over 3 μm^2/s with moderate excitation intensities.**

I. Introduction

Over the past decade, single molecule spectroscopy and imaging has given researchers tremendous insight into various biological phenomena. Some notable results include the study of influenza [1], hepatitis B [2], and molecular motors [3]. Most single particle methods rely on wide-field imaging using charge coupled device (CCD) cameras. Despite their successes to date, this reliance limits the achievable sensitivity as well as the spatial and temporal resolution, especially when studying single particles inside living cells.

To alleviate the inherent problems of wide-field detection, several alternative methods have been developed. One such approach split a laser into two beams, focused each beam onto separate focal planes, and rotated the beams about a small circle [4]. When a particle was "locked" near the center of the circle, the position of the particle could be inferred using lock-in demodulation of the measured fluorescence intensity. The position estimate was used to regulate the position of a three-axis nanopositioning stage to keep the particle close to the center of the circle. Other techniques use the same principle of servoing about a position estimate but have different methods for localizing the particle. For example, earlier work by one of the authors (with others) took several intensity measurements in a constellation pattern and used GPS-like localization to calculate the position of the particle [5]. Two other methods use multiple photon detectors to determine the position of the particle [6], [7]. All of these techniques have demonstrated the ability of tracking diffusing particles with coefficients between 0.1 and 20 μm^2/s at various signal-to-noise ratios (SNRs). These techniques, however, either directly or indirectly measure the displacement of the particle, thereby leading to costly optics, complicated configurations, or temporal inefficiencies.

In light of these concerns, a three-dimensional nonlinear reactive tracking algorithm was developed in [8] that avoids real-time localization while forcing the trajectory of the excitation volume to converge to a volume around the particle. The algorithm avoids temporal inefficiencies and is versatile in the fact that it can be implemented on any device that serially acquires measurements of any three-dimensional scalar potential field of arbitrary shape (e.g. magnetic force [9], multiphoton, and stimulated emission depletion microscopy). Since the particle position is not measured in real-time, a variety of techniques can be employed to analyze the experimental data and determine particle trajectories and statistical information. In this paper, we use the fluoroBancroft estimation algorithm introduced by one of the authors [10] to estimate the particle position and then analyze the resulting trajectories to determine diffusion coefficients.

II. Experimental Setup

Our experimental setup, illustrated in Fig. 1, consisted of a standard epi-fluorescence confocal microscope built upon an inverted microscope (Axiovert 200, Carl Zeiss). A 488 nm laser (FiberTec II, Blue Sky Research) was directed through a beam expander and onto a dichroic filter (T495LP, Chroma) which reflected the beam onto the back aperture of an objective lens (water immersion, 63x, 1.2 N.A. C-Apochromat, Carl Zeiss). The objective lens focused the beam to a diffraction-limited spot onto the sample. A three-axis piezoelectric nanopositioning stage (Nano-PDQ, Mad City Labs), driven by a high-voltage amplifier (Nano-Drive 85, Mad City Labs), carried the sample and provided 50 μm of fine displacement in each axis. The fluorescence emitted by the sample was collected by the objective lens and passed through the dichroic filter and a bandpass filter (HQ625/30m, Chroma). The output signal was then split into two beams by a beamsplitter which focused a fraction R (33%) onto a CCD camera (Retiga EXi, QImaging). The remaining signal was focused through a 25 μm pinhole onto an avalanche photodiode (APD) (SPCM-AQR-14, Perkin Elmer). The tracking algorithm was implemented on a CompactRIO (cRIO-9076, National Instruments), consisting of a field programmable gate array (FPGA), a real-time processor, a 16-bit 100 kHz analog input module (NI 9215), a 16-bit 100 kHz analog output module (NI 9263), and a digital input/output module (NI 9401). The analog input module measured stage position feedback and the analog output module commanded an actuation voltage to the stage amplifier. The digital input/output

978-1-4673-2064-1/12/$31.00 ©2012 IEEE

module was connected to the digital output of the APD.

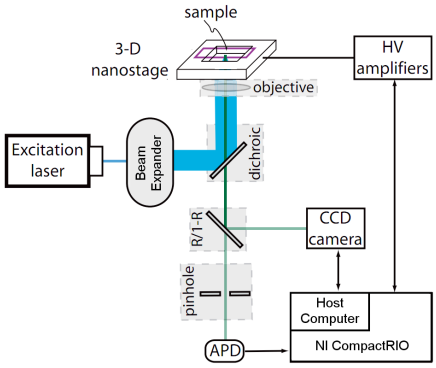

Fig. 1. Diagram of confocal microscope used in the tracking experiments. The excitation laser (thick blue line) was focused by an objective lens into the sample. Fluorescence (thin green line) generated by beam/sample interactions was passed through the objective and the dichroic. A beam splitter reflected a fraction R of the fluorescent light to a CCD camera and passed the remaining light to the pinhole. The light focused onto the pinhole was detected by an avalanche photodiode. The sample was displaced by a three-axis piezoelectric nanostage and the tracking algorithm was implemented on a National Instruments CompactRIO.

III. Tracking Algorithm

Recall that a confocal microscope uses a diffraction-limited excitation source to illuminate points of a fluorescently-labeled specimen. When imaging a particle much smaller than the diffraction limit (i.e. a point source), the spatial intensity pattern formed at the detector is the point spread function (PSF) of the microscope. Although an analytical expression for the PSF can be derived [11], it is difficult to incorporate into real-time control algorithms due to its complexity. Consequently, our algorithm treats the PSF as an unknown scalar potential field and therefore assumes very little knowledge of the underlying structure. An important feature of an aberration-free PSF utilized by the algorithm is the existence of a maximum when the focus of the laser is perfectly centered on the particle. The algorithm, (2) below, adds artificial non-holonomic constraints to the motion of the nanopositioning stage and drives the trajectories to a volume around the maximum provided a sufficiently large signal-to-noise ratio (SNR). As shown in Fig. 2, the algorithm consists of two components: a slow outer loop for position command generation and a fast inner loop for stage position actuation.

The outer loop generates desired position commands based on the change in the measured intensity along the trajectory. It is described briefly below; details can be found in [8]. Let the desired velocities of the (x,y,z) stages respectively be

$$u = \begin{pmatrix} u_x & u_y & u_z \end{pmatrix}^T. \tag{1}$$

Given the intensity $I(t)$, the discrete-time control law is given by

$$\theta(t) = \theta(t-\Delta t) + \frac{v}{r}\left(\Delta t - K\Delta I(t)\right), \tag{2a}$$

$$\phi(t) = \phi(t-\Delta t) + \omega_z \Delta t, \tag{2b}$$

$$\Delta I(t) = I(t) - I(t-\Delta t), \tag{2c}$$

$$\begin{pmatrix} u_x(t) \\ u_y(t) \\ u_z(t) \end{pmatrix} = v \begin{pmatrix} \cos\theta(t) \\ \sin\theta(t)\cos\phi(t) \\ -\sin\theta(t)\sin\phi(t) \end{pmatrix} \tag{2d}$$

The control law has several tunable parameters, including the control update period Δt, the proportional gain K, the $y-z$ plane rotation rate ω_z, the speed v, and the nominal radius r. All parameters are assumed to be strictly positive.

Although not apparent in (2), the intensity accumulation time significantly affects the likelihood of convergence in the presence of measurement noise. For example, short accumulation times reduce the SNR and better approximate a point-measurement, whereas longer accumulation times increase SNR but represent an average over a sweep of positions. The choice of accumulation time reflects the unavoidable tradeoff between speed and sensitivity and is common to all particle tracking algorithms.

Lastly, the stages must follow the commanded trajectories with sufficiently small error, so, assuming sufficient SNR in the intensity measurements, the minimum bandwidth of the inner loop ultimately determines the quality of tracking.

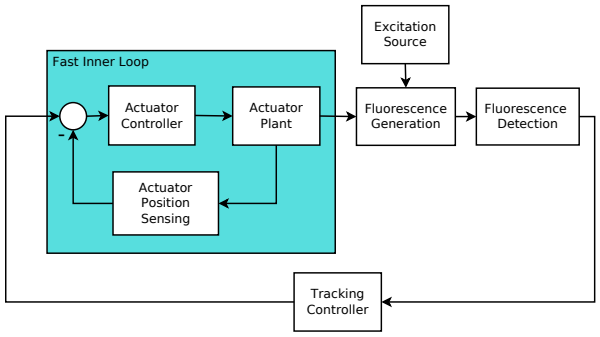

Fig. 2. High-level block diagram of the tracking algorithm. The tracking controller generates position commands based on changes in intensity. The fast inner loop responds to position commands generated by the tracking controller.

The outer loop assumes the positioning stages follow the commanded signals faithfully. Thus, tracking performance is limited by the closed-loop bandwidths of the stages. To reduce tracking error at higher frequencies, a custom feedback controller was designed and implemented in the FPGA on the CompactRIO.

System identification of each stage was performed by measuring the plant frequency responses through random excitation. A pseudorandom binary sequence with a 0.01 V amplitude was driven into each stage and position feedback was measured at a rate of 100 kHz. The position feedback signal was assumed to be corrupted by noise, so the H_1 estimator was calculated using Bartlett's method [12].

Given these frequency responses, a controller was designed for each stage using loop shaping principles. To reduce quantization noise, which is especially prevalent in fixed-point systems, a low-order controller structure was

chosen and consisted of a gain, a pure integrator, and two first-order low-pass filters. Further, dynamic coupling was assumed to be negligible given the "frame-in-frame" design of the stages. The corner frequencies of the low-pass filters were chosen to robustly attenuate the high-frequency resonances and the gains were selected to set the open loop crossover frequencies. Each feedback controller was shaped in continuous-time and discretized for a sampling frequency of 100 kHz using the bilinear transform. The resulting bandwidths of the complementary sensitivities were (800, 200, 100) Hz in (x,y,z), respectively. Frequency responses detailing stability and performance are shown in Fig. 3.

IV. Localization of a Diffusing Particle

Since the control law is reactive in nature it does not track by localizing position. While this leads to a simple algorithm that is tunable to perform well at different intensities, SNRs, and rates of dynamics, it does mean that position must be inferred from the data. One approach of analyzing tracking performance is to estimate the particle trajectories using offline localization. Since the measurements are intensities along a 3-D trajectory, rather than images, fitting techniques common to wide-field approaches such as Gaussian fitting [13] or maximum likelihood [14] are not applicable. We turn instead to the fluoroBancroft (FB) algorithm developed by one of the authors [10]. This approach provides an analytical solution to the estimation problem using as few as four non co-planar measurements. The FB algorithm approximates the PSF as a Gaussian function with parameters σ_x, σ_y, σ_z, corresponding to the spread widths. From the results derived in [15], we assume

$$\sigma_x = \sigma_y = \frac{\sqrt{2}\lambda}{2\pi\,(\text{N.A.})}, \quad \sigma_z = \frac{2\sqrt{6}n\lambda}{2\pi\,(\text{N.A.})^2}, \tag{3}$$

where λ is the fluorescence wavelength, N.A. is the numerical aperture of the lens, and n is the refractive index of the immersion fluid.

The position of a diffusing particle $x_p \in \mathbb{R}^3$ sampled at time step δt can be modeled by the first-order stochastic difference equation

$$x_p[k+1] = x_p[k] + \sqrt{2D(\delta t)}w[k], \tag{4}$$

where D is the diffusion coefficient and $w[\cdot]$ is a Gaussian white noise process with unit variance and zero mean. To estimate the position of the particle in time, we assume the particle is moving slowly relative to the motion of the stages and apply the FB algorithm to a finite set of sequential measurements. In other words, for a measurement vector consisting of intensity and corresponding stage positions $\gamma[k] = (I[k] \quad x[k] \quad y[k] \quad z[k])^T$, we estimate the particle position $\hat{x}_p[k]$ by applying the FB algorithm to the set $\{\gamma[k], \gamma[k+1], \ldots, \gamma[k+N-1]\}$, where N is the FB window length. Elements with intensities less than or equal to the mean of the background noise are discarded. When used in this manner, the FB algorithm behaves like a low-pass filter with N inversely proportional to the cut-off frequency. Thus, N should be maximized to yield a large SNR yet chosen small enough so that the particle does not move significantly within the time period. The estimated particle positions are smoothed using a Rauch-Tung-Striebel (RTS) smoother [16] and the mean square displacement (MSD) is calculated [17]. The FB window length and the RTS process variance Q are adjusted until the MSD of the estimated particle position is approximately linear. Recall that for a particle undergoing pure diffusion the MSD is linear with respect to time. The diffusion coefficient is then estimated by fitting a line to a portion of the MSD.

V. Experimental Results

In this section, we present experimental results of the tracking algorithm when applied to diffusing quantum dots (QD625, Life Technologies) in solutions of differing viscosities. Samples were prepared by diluting quantum dots in deionized water and by adding different proportions of glycerol.

A. Tracking a Fixed Particle

To obtain a fixed quantum dot, a 9:1 solution of glycerol to water was created and dried onto a cover slip. The cover slip was adhered to a microscope slide and mounted onto the stage. A fixed quantum dot was found using the CCD and the tracking algorithm was enabled. The control update rate was set to 2 kHz and the APD accumulation time was set to 500 μs. The velocity v was 10 μm/s and the steady-state radius r was 20 nm, corresponding to 75 rev/s around the steady-state circle. The radius was chosen small relative to the width of the PSF (calculated below) to yield high sensitivity and the velocity was chosen to yield a rotational frequency large enough so the circle was traversed in minimal time yet small enough that the stages could follow the trajectory. The speed of the rotating plane ω_z was 30 rev/s and the gain K was 0.1, both of which were adjusted experimentally. The laser power was approximately 4 mW.

Fig. 4 shows the x and z traces for a typical run. (The trace in the y–axis was nearly identical to that in x and was omitted for space reasons.) The intensity was regulated to 38 ± 6 counts/500 μs, representing the mean and standard deviations. The standard deviation matches what one would expect for shot noise. The position of the quantum dot was estimated by the procedure described in Sec. IV. Since the quantum dots fluoresce with a wavelength of 625 nm, the FB parameters were chosen to be $\sigma_x = \sigma_y = 117$ nm and $\sigma_z = 451$ nm. The mean background noise η_B was measured to be 0.1 counts/500 μs when no quantum dot was present. The FB window length was 500 points (corresponding to 250 ms), the RTS process noise variance Q was 0.01 μm^2, and the measurement noise variance R was unity. These parameters were adjusted until the trajectories were adequately smoothed.

Correlation between the (x,y) trajectories was observed, indicating the presence of a non-random disturbance such as mechanical or sensor drift due to a lack of thermal regulation or fluidic flow caused by laser-induced heating. Moreover, the z trajectory appeared significantly different from the x

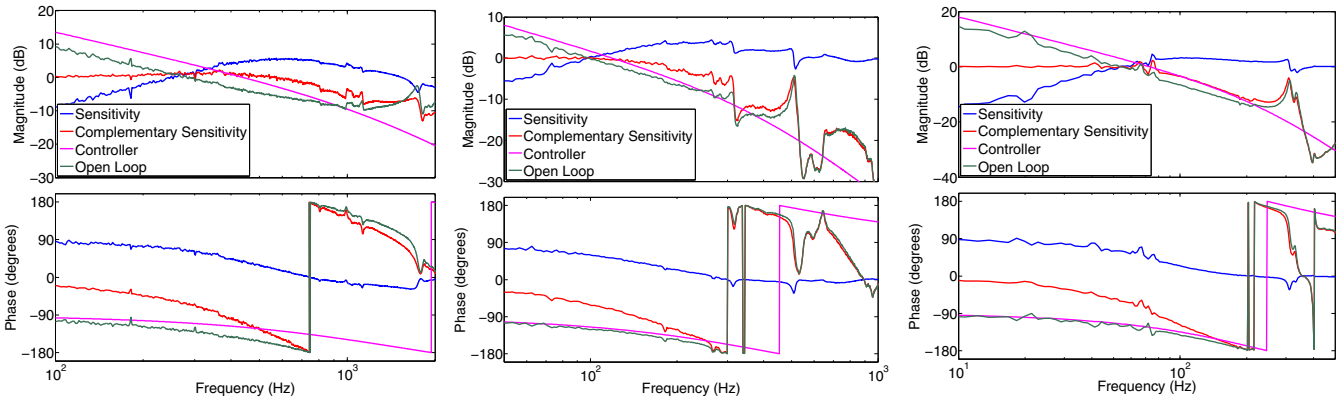

(a) X Stage Bode Plot (b) Y Stage Bode Plot (c) Z Stage Bode Plot

Fig. 3. Frequency responses for the (x,y,z) stages. Discrete-time linear feedback controllers were designed for each stage using loop-shaping principles and were implemented in an FPGA at a 100 kHz update rate. The bandwidths of the complementary sensitivity functions (shown in red) were approximately $(800, 200, 100)$ Hz in (x,y,z), respectively.

trajectory due to the small commanded radius which implies that most of the measurements were observed in the (x,y) plane. As such, there was larger uncertainty in z.

B. Tracking Diffusing Particles

To determine how well the controller could track a slowly diffusing particle, a small amount of the previously mentioned 9:1 solution was placed into a multiwell microscope slide, sealed with a cover slip, and mounted to the stage. A diffusing dot was located with the CCD and the tracking algorithm was turned on. The control update rate was set to 5 kHz and the APD accumulation time was set to 200 μs. The velocity v was 750 μm/s and the steady-state radius r was 637 nm, corresponding to 187.5 rev/s around the steady-state circle. The radius was chosen to enlarge the search space of the controller and the velocity was chosen to set the nominal rotational frequency. The chosen rotational frequency surpassed the bandwidth of the z stage, but tracking was maintained at the cost of reducing the effective radius in z. The speed of the rotating plane ω_z was 137.5 rev/s and the gain K was 0.4, both of which were chosen experimentally. The laser power was approximately 4 mW.

The results are shown in Fig. 5. The stages tracked the particle for more than 20 s with an average intensity of 2 counts/200 μs. The experiment had ended before tracking was lost. Although the average intensity was low, the maximum observed intensity was over 80 counts/200 μs. This discrepancy is due to the large radius and short accumulation time. The position of the quantum dot was estimated as described in the previous subsection. The mean background noise was measured to be approximately zero and was neglected. The window length was 150 points (corresponding to 30 ms), the RTS process noise variance was $2{\cdot}10^{-6}$ μm^2, and the measurement noise variance was unity. These parameters were adjusted to yield linearity in the MSD. A linear fit to the MSD yielded a diffusion coefficient of 0.24 μm^2/s. Since the commanded radius was chosen much larger than the assumed PSF widths, estimation errors occurred because the PSF is not truly Gaussian at large distances from the center of the particle. In addition, a relatively low SNR and a suboptimal measurement constellation [18] resulted in noisy position estimates.

To stress the tracking algorithm and explore the limit on faster particles, a new 5:1 solution of glycerol to water was made and prepared as described in the previous section. The control update rate was set to 10 kHz and the APD accumulation time was set to 100 μs. The velocity v was 750 μm/s and the steady-state radius r was 1.193 μm, corresponding to 100 rev/s around the steady-state circle. The speed of the rotating plane ω_z was 45 rev/s and the gain K was 10, both of which were selected experimentally. To improve the SNR, the laser power was increased to approximately 20 mW. The resulting trajectories are shown in Fig. 6. The stages tracked the quantum dot for more than 5 s with an average intensity of 0.3 counts/100 μs. Again, the experiment ended before tracking failed. The position of the quantum dot was estimated as previously described. The mean background noise was measured to be approximately zero and was neglected. The window length was 150 points (corresponding to 15 ms), the RTS process noise variance was 10^{-5} μm^2 and the measurement variance was 1. A line fit to the MSD yielded a diffusion coefficient of 3.7 μm^2/s. The FB estimates were noisier due to the increased radius and the decreased accumulation time. As such, the uncertainty in the position estimates, and therefore the diffusion coefficient, was significant.

VI. Discussion

Given the results detailed in Sec. V, it is evident that the control law tracks diffusing quantum dots with very little information about the PSF. Moreover, the sensitivity and speed of the controller can be adjusted using intuitive parameters. For example, the controller used to track the fixed quantum dot was tuned for high-sensitivity with a small radius of 20 nm and a long accumulation time of 500 μs. This allowed the controller to stay very close to

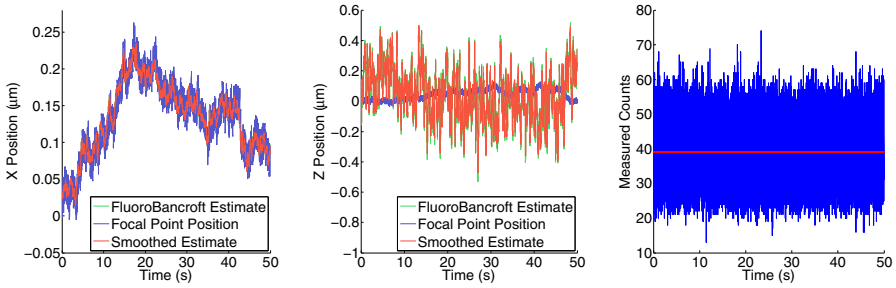

(a) X Position (b) Z Position (c) Measured Intensity

Fig. 4. Tracking run with a fixed particle. Plots (a)-(b) show (x,z) stage trajectories (blue), fluoroBancroft estimates of the particle (green), and smoothed fluoroBancroft estimates (red). The y trajectory was nearly identical to x and was therefore omitted. Plot (c) shows the measured intensities in counts/500 μs. The controller regulated the intensity to 38$\pm$6 counts/500 μs with the mean indicated by the solid red line in (c).

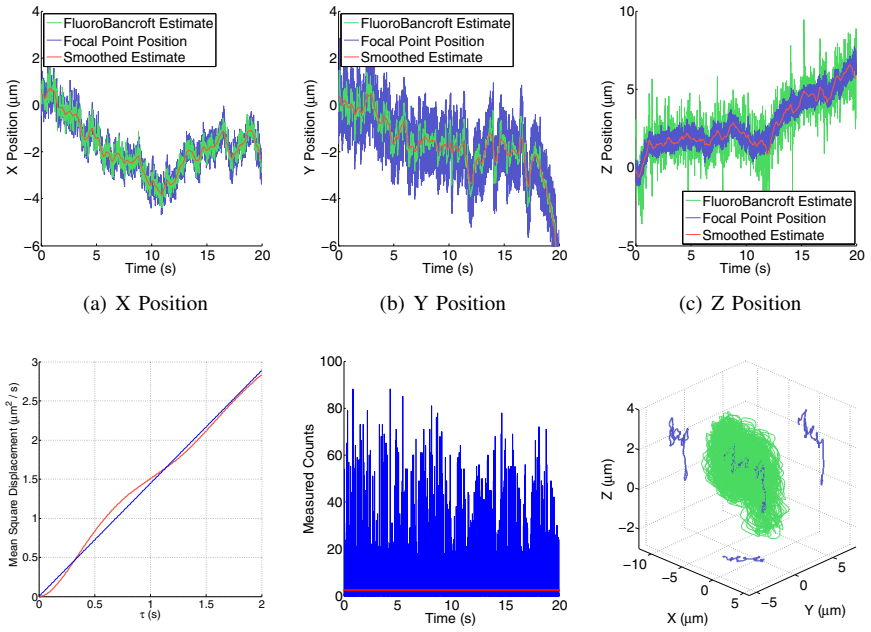

(a) X Position (b) Y Position (c) Z Position

(d) Mean Square Displacement (e) Measured Intensity (f) Trajectory

Fig. 5. Tracking run with a slowly diffusing particle. Plots (a)-(c) show stage trajectories (blue), fluoroBancroft estimates of the particle (green), and smoothed fluoroBancroft estimates (red center line). Plot (f) shows a 3-D image of the stage trajectories (green) and the smoothed positions (blue, with projections onto respective planes). Plot (e) shows the measured intensities with an average (indicated by the red line) of 2 counts/200 μs. The mean square displacement is shown in (d) as a red curve with corresponding linear fit (blue) indicating a diffusion coefficient of 0.24 μm^2/s.

the maximum of the PSF. The other controllers were tuned for high-speed with larger radii and shorter accumulation times. Although we showed the controller tracking a quantum dot diffusing at 3.7 μm^2/s, it is unknown whether this is an upper limit. A rigorous understanding of stability and performance could yield optimal parameters for improved tracking. Further, since the outer loop assumes the inner loop faithfully follows the command signals, more accurate tracking could be achieved by raising the bandwidth of the inner loop. This could be done by implementing more advanced feedback or feedforward controllers or by using faster actuators.

Although the controller avoids temporal inefficiencies by not directly estimating the position of the particle, calculation of diffusion coefficients must be performed offline using stage trajectories and intensities. Here we used the FB algorithm to estimate the particle positions. The choice of window length in the estimation is essential as choosing it too short leads to noisy estimates while choosing it too long leads to a low-pass filtering effect and thus an under-reporting of the diffusion coefficient. It is possible that better estimation can be achieved by optimizing the scan parameters with such estimation in mind, possibly while sacrificing some tracking speed. A different approach is to take advantage of the residual fluctuations in the measured intensity as these encode information about the correlation statistics of the particle. This approach has been developed successfully under a different tracking scheme and allows for a direct computation of the diffusion coefficient without ever estimating the actual particle position [19].

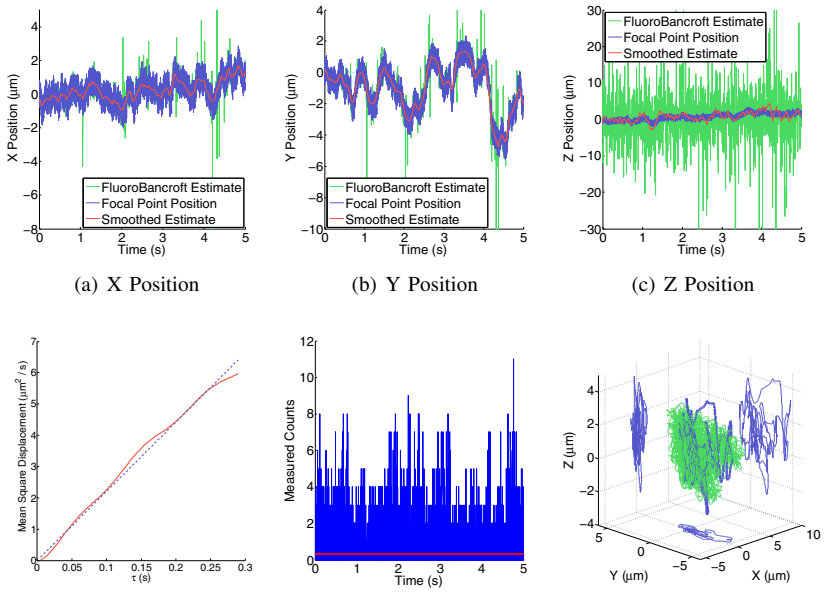

(a) X Position (b) Y Position (c) Z Position

(d) Mean Square Displacement (e) Measured Intensity (f) Trajectory

Fig. 6. Tracking run with a quickly diffusing particle. Plots (a)-(c) show stage trajectories (blue), fluoroBancroft estimates of the particle (green - noisy lines), and a smoothed fluoroBancroft estimate (red center line). Plot (f) shows a 3-D image of the stage trajectories (green) and the smoothed estimates (blue, with projections onto respective planes). Plot (e) shows the measured intensities with an average (indicated by the red line) of 0.3 counts / 100 μs. The mean square displacement is shown in (d) as a red curve with corresponding linear fit (blue) indicating a diffusion coefficient of 3.7 μm^2/s.

VII. Conclusion

In this paper we demonstrate the effectiveness of a nonlinear reactive control law that tracks particles in three dimensions. Experimental results indicate the controller is capable of tracking diffusing quantum dots on a standard confocal microscope without directly estimating the position of the particle and without any *a priori* knowledge of the optical setup. Since the particle position is not used by the controller, performance validation and diffusion statistics can be calculated offline by analyzing the resulting trajectories and intensities. Moreover, the controller can be tuned for different sensitivities and speeds, thereby increasing its effectiveness of tracking particles in various conditions.

VIII. Acknowledgements

This work was supported in part by NSF through grant CMMI-0845742.

References

[1] S.-L. Liu, Z.-L. Zhang, Z.-Q. Tian, H.-S. Zhao, H. Liu, E.-Z. Sun, G. F. Xiao, W. Zhang, H.-Z. Wang, and D.-W. Pang, "Effectively and efficiently dissecting the infection of influenza virus by quantum-dot-based single-particle tracking," *ACS Nano*, vol. 6, no. 1, pp. 141–150, 2012.

[2] X. Hao, X. Shang, J. Wu, Y. Shan, M. Cai, J. Jiang, Z. Huang, Z. Tang, and H. Wang, "Single-particle tracking of hepatitis B virus-like vesicle entry into cells," *Small*, vol. 7, no. 9, pp. 1212–1218, 2011.

[3] E. J. G. Peterman, H. Sosa, and W. E. Moerner, "Single-molecule fluorescence spectroscopy and microscopy of biomolecular motors," *Annu. Rev. Phys. Chem*, vol. 55, pp. 79–96, 2004.

[4] K. McHale, A. J. Berglund, and H. Mabuchi, "Quantum dot photon statistics measured by three-dimensional particle tracking," *Nano Lett.*, vol. 7, no. 11, pp. 3535–3539, 2007.

[5] Z. Shen and S. B. Andersson, "3-D tracking of fluorescent nanoparticles in a confocal microscope," in *Proc. of the IEEE Conf. on Decision and Control*, 2011, pp. 5856–5861.

[6] H. Cang, C. S. Xu, D. Montiel, and H. Yang, "Guiding a confocal microscope by single fluorescent nanoparticles," *Opt. Lett.*, vol. 32, no. 18, pp. 2729–2732, 2007.

[7] N. P. Wells, G. A. Lessard, and J. H. Werner, "Confocal, three-dimensional tracking of individual quantum dots in high-background environments," *Anal. Chem.*, vol. 80, no. 24, pp. 9830–9834, 2008.

[8] S. B. Andersson, "A nonlinear controller for three-dimensional tracking of a fluorescent particle in a confocal microscope," *Appl. Phys. B*, vol. 104, no. 1, pp. 161–173, 2011.

[9] D. Baronov and S. B. Andersson, "Controlling a magnetic force microscope to track a magnetized nanosize particle," *IEEE T. Nanotechnol.*, vol. 9, no. 3, pp. 367–374, 2010.

[10] S. B. Andersson, "Localization of a fluorescent source without numerical fitting," *Opt. Expr.*, vol. 16, no. 23, pp. 18 714–18 724, 2008.

[11] J. E. Jonkman and E. H. K. Stelzer, *Resolution and Contrast in Confocal and Two-Photon Microscopy*. Wiley-Liss, 2002, pp. 101–125.

[12] J. S. Bendat and A. G. Piersol, *Random Data: Analysis and Measurement Procedures*, 3rd ed. Wiley, 2000, pp. 189–217.

[13] R. E. Thompson, D. R. Larson, and W. W. Webb, "Precise nanometer localization analysis for individual fluorescent probes," *Biophys. J.*, vol. 82, no. 5, pp. 2775–2783, 2002.

[14] K. I. Mortensen, L. S. Churchman, J. A. Spudich, and H. Flyvbjerg, "Optimized localization analysis for single-molecule tracking and superresolution microscopy."

[15] B. Zhang, J. Zerubia, , and J.-C. Olivo-Marin, "Gaussian approximations of fluorescence microscope point-spread functions," *Appl. Opt.*, vol. 46, no. 10, pp. 1819–1829, 2007.

[16] D. Simon, *Optimal State Estimation: Kalman, H Infinity, and Nonlinear Approaches*. Hoboken: John Wiley and Sons, 2006, pp. 286–294.

[17] M. J. Saxton and K. Jacobson, "Single-particle tracking: applications to membrane dynamics," *Ann. Rev. Biophys. Biomol. Struct.*, vol. 26, pp. 373–399, 1997.

[18] Z. Shen and S. B. Andersson, "Optimal measurement constellation of the fluorobancroft localization algorithm for position estimation in tracking confocal microscopy," *Mechatronics*, 2011. *In press.*

[19] A. J. Berglund and H. Mabuchi, "Tracking-FCS: fluorescence correlation spectroscopy of individual particles," *Opt. Expr.*, vol. 13, no. 20, 2005.